Supplement of

Assessment of WRF-GHG model simulations during the CAFE-Brazil Campaign in Amazonia

Noelia Rojas Benavente et al.

Correspondence to: Noelia Rojas Benavente (rnoeliab@gmail.com)

A Sensitivity analysis of the WRF model

The Brazilian National Institute of Meteorology (INMET) operates an extensive network of meteorological stations across Brazil, providing essential data for weather forecasting, climate monitoring, and environmental research (Moura et al., 2016). These stations record key atmospheric variables such as temperature, humidity, precipitation, wind speed, and surface pressure. In this study, observations from 99 INMET stations located within the WRF-GHG model's intermediate domain (D02) were used to evaluate near-surface meteorological conditions (see Table S1 and Fig. 1a, from main paper). These stations provide valuable spatial coverage over the central and northern Amazon, enabling a robust comparison between model simulations and ground-based measurements.

Given the wide spatial distribution of INMET stations across Brazil, both observed and simulated meteorological data were grouped and averaged across four defined regions (see Fig. 1a, from main paper). This subsection presents a sensitivity analysis of the WRF (Weather Research and Forecasting) model, aimed at understanding the impact of various model configurations on the simulation of atmospheric conditions, particularly in the context of greenhouse gas (GHG) concentrations such as CO_2 and CH_4. Sensitivity analyses are critical in assessing how different parameterizations and input conditions influence model performance, especially for complex, large-scale simulations like those used in atmospheric modeling over the Amazon region.

Table S 1: INMET Stations distributed over our analysis domain.

Region	Stations	Latitude	Longitude	T_{2m}	RH_{2m}	WS_{10m}	WD_{10m}	Region	Stations	Latitude	Longitude	T_{2m}	RH_{2m}	WS_{10m}	WD_{10m}
	Autazes	-3.58	-59.12	X	X	X	X		Belen	-1.41	-48.43	X	X	X	X
	Barcelos	-0.98	-62.92	X	X	X	X		Breves	-1.68	-50.47	X	X	X	X
	Coari	-4.09	-63.14	X	X	X	X		Cameta	-2.23	-49.49	X	X	X	X
	Itacoatiara	-3.13	-58.48	X	X	X	X		Itaubal	0.56	-50.82	X	X	X	X
	Itaituba	-4.27	-55.99	X	X	X	X		Macapa	0.03	-51.08	X	X	X	X
	Manacapuru	-3.29	-60.62	X	X	X	X	R2	Oiapoque	3.81	-51.86	X	X	X	X
	Manaus	-3.10	-60.01	X	X	X	X		Porto de Moz	-1.82	-52.11	X	X	X	X
	Maues	-3.39	-57.67	X	X	X	X		Porto Grande	0.69	-51.40	X	X	X	X
R1	Monte Alegre	-2.0	-54.07	X	X	X	X		Soure	-0.72	-48.51	X	X	X	X
	Obidos	-1.88	-55.51	X	X	X	X		Tome Acu	-2.59	-48.36	X	X	X	X
	Parintins	-2.63	-56.75	X	X	X	X		Altamira	-3.27	-52.39	X	X	X	X
	Placas	-3.86	-54.21	X	X	X	X		Araguaina	-7.10	-48.20	X	X	X	X
	Presidente Figueiredo	-2.05	-60.02	X	X	X	X		Araguatins	-5.64	-48.11	X	X	X	X
	Rio Urubu	-2.63	-59.60	X	X	X	X		Colinas	-8.09	-48.47	X	X	X	X
	G. Da Cachoeira	-0.12	-67.06	X	X	X	X		Conceicao do Araguaia	-8.30	-49.28	X	X	X	X
	Santarem	-2.50	-54.72	X	X	X	X		Maraba	-5.36	-49.05	X	X	X	X
	Urucara	-2.53	-57.75	X	X	X	X		Marianopolis	-9.57	-49.72	X	X	X	X
	Apiacas	-9.56	-57.39	X	X	X	X		Medicilandia	-3.51	-52.96	X	X	X	X
	Apui	-7.20	-59.88	X	X	X	X		Novo Repartimento	-4.24	-49.93	X	X	X	X
	Ariquemes	-9.94	-62.96	X	X	X	X		Pacaja	-3.84	-50.63	X	X	X	X
	Boca do Acre	-8.77	-67.33	X	X	X	X	R4	Pedro Afonso	-8.96	-48.17	X	X	X	X
	Carlinda	-9.97	-55.82	X	X	X	X		Redencao	-8.04	-50.00	X	X	X	X
	Cotriguagu	-9.90	-58.57	X	X	X	X		Rondon do Para	-4.82	-48.17	X	X	X	X
	Eirunepe	-6.65	-69.86	X	X	X	X		Santa Fe do Araguaia	-7.12	-48.78	X	X	X	X
	Guaranta Do Norte	-9.95	-54.89	X	X	X	X		Santa Maria Das Barreiras	-8.72	-49.85	X	X	X	X
R3	Humaita	-7.55	-63.07	X	X	X	X		Santana do Araguaia	-9.33	-50.35	X	X	X	X
	Labrea	-7.26	-64.78	X	X	X	X		Sao Feliz do Xingu	-6.63	-51.95	X	X	X	X
	Manicore	-5.78	-61.28	X	X	X	X		Serra dos Carajas	-6.07	-50.14	X	X	X	X
	Mina do Palito	-6.31	-55.78	X	X	X	X		Tucuma	-6.74	-51.14	X	X	X	X
	Novo Aripuana	-8.09	-60.38	X	X	X	X		Tucurui	-3.82	-49.67	X	X	X	X
	Parque Estadual Chandless	-9.35	-69.92	X	X	X	X		Xinguara	-7.11	-49.92	X	X	X	X
	Porto Velho	-8.79	-63.84	X	X	X	X								
	Rio Branco	-9.67	-68.16	X	X	X	X								

The value "x" represents the existence of meteorological variables available for each station.

The WRF-GHG model's surface meteorological outputs were compared to hourly data from 99 INMET stations across four Brazilian climate regions (Fig. S1). The model reproduces the diurnal cycles of T_{2m} and RH_{2m} well, with

the WGY-Test configuration slightly outperforming the MGM-Test. Wind speed shows more variability, with both under- and overestimations, but overall trends are preserved. Wind direction, however, remains challenging to model due to sensitivity to local turbulence and topography. A Taylor diagram (Fig. S2) shows strong correlations ($R \leq 0.95$) for temperature and humidity, with WGY-Test slightly outperforming MGM-Test in most regions. Wind speed correlations are weaker ($R \leq 0.6$), though WGY-Test offers slight improvement over MGM-Test.

Table S 2: Physical scheme in WRF-GHG model for sensitivity analysis.

Physical scheme	**WGY-Test**	**MGM-Test**
Microphysics scheme	Morrison 2-moment Scheme	WRF Single-moment 6-class Scheme
Cumulus parameterization	Grell 3D Ensemble Scheme	Grell-Devenyi Ensemble Scheme
Planetary boundary scheme	Mellor-Yamada-Janjic Scheme	Yonsei University Scheme
Short-wave and Long-wave radiation scheme	CAM Schemes	RRTMG Schemes
Land surface model	Unified Noah Land Surface	Unified Noah Land Surface
Surface Layer	Revised MM5	Revised MM5

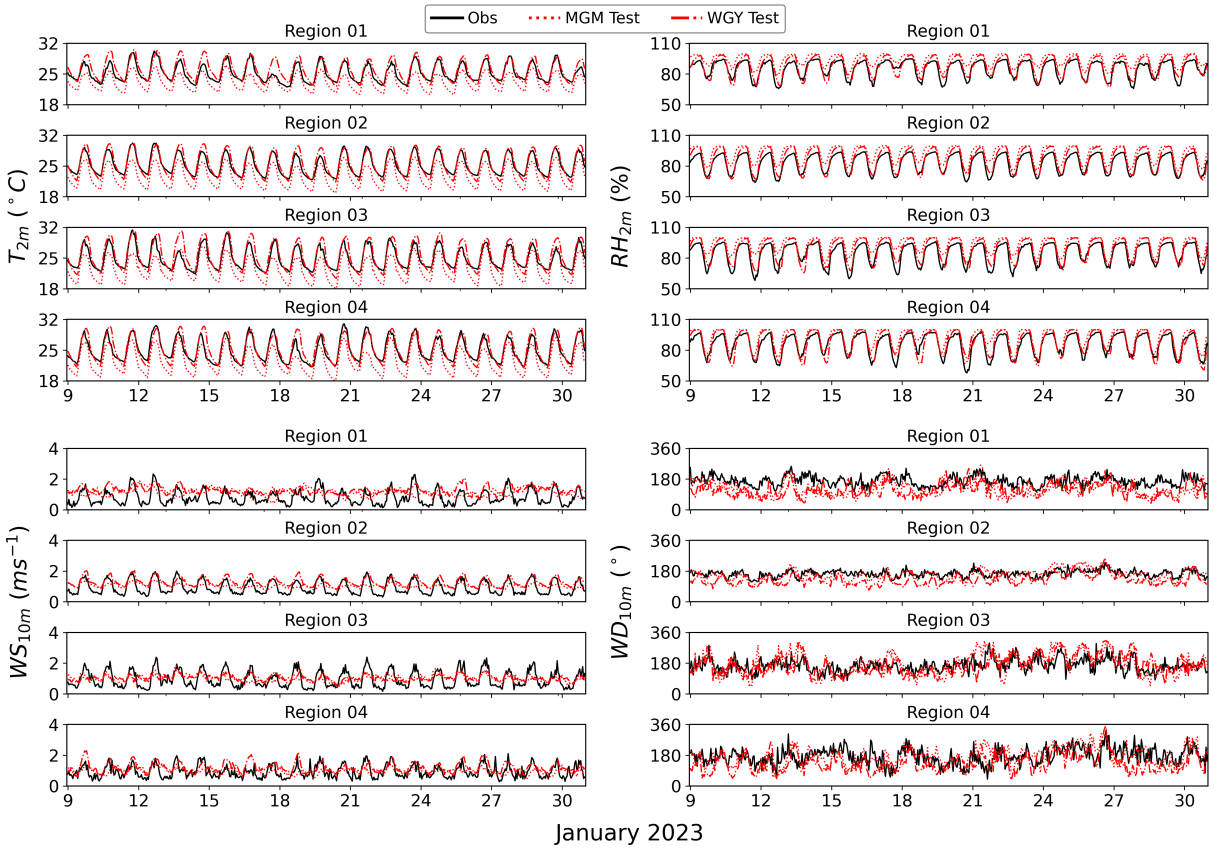

Figure S 1: Time series comparison of observed (Obs) and modeled meteorological variables from two WRF simulations (MGM Test - red dotted line; WGY Test - red dashed line) across four regions during January 2023. Variables include 2-meters air temperature (T_{2m}, °C), 2-meters relative humidity (RH_{2m}, %), 10-meters wind speed (WS_{10m}, m/s), and 10-meters wind direction (WD_{10m}, °)

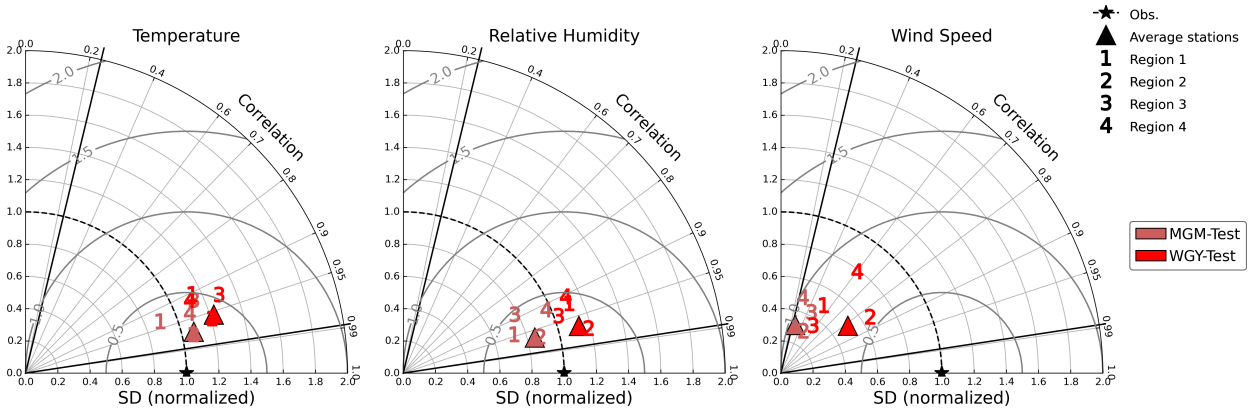

Figure S 2: Taylor diagram depicting the performance of the WRF-GHG simulations (MGM-Test and WGY-Test) in comparison with INMET stations across the four selected regions. The diagram highlights the correlation, standard deviation, and overall model efficiency in relation to the observed data for temperature, relative humidity, and wind speed.

B Figures and Tables

B.1 WRF meteorological evaluation

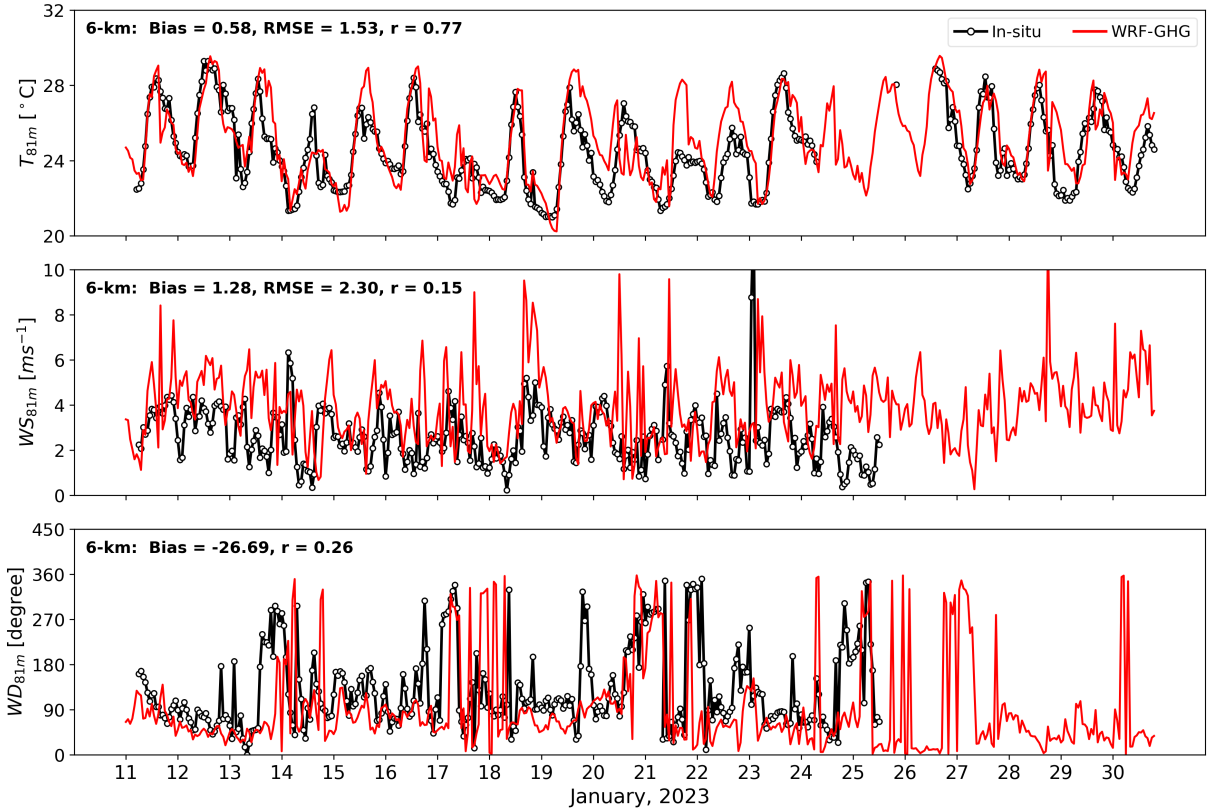

Figure S 3: Time series comparison of observed and modeled meteorological variables at the ATTO site (Amazon Tall Tower Observatory) during January 2023. Variables include 81-meters air temperature (T_{81m}, °C), 81-meters wind speed (WS_{81m}, m/s), and 81-meters wind direction (WD_{81m}, °).

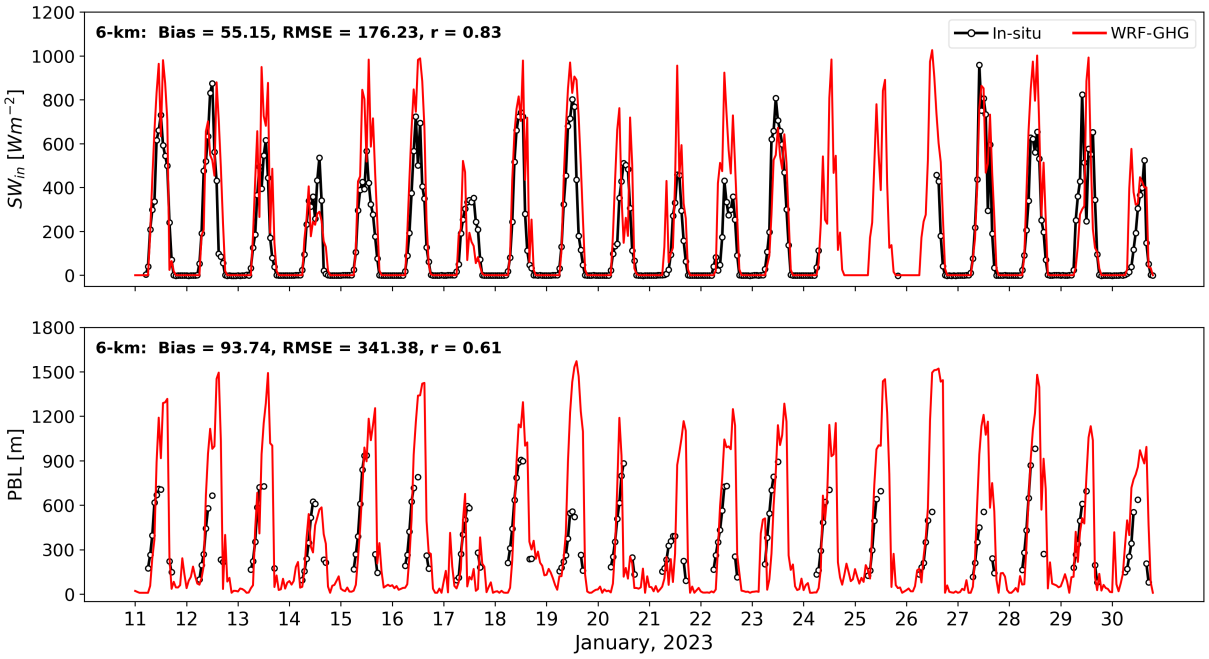

Figure S 4: Time series comparison of observed and modeled meteorological variables at the ATTO site (Amazon Tall Tower Observatory) during January 2023. Variables include radiation (SW_{81m}, Wm^{-2}) and Planetary Boundary Layer (PBL, m).

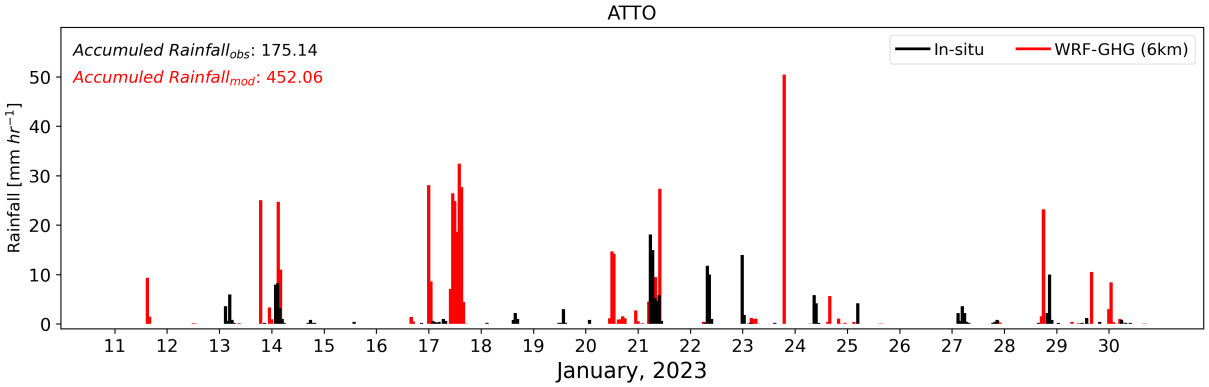

Figure S 5: Time series comparison of observed and modeled precipitation at the ATTO site (Amazon Tall Tower Observatory) during January 2023.

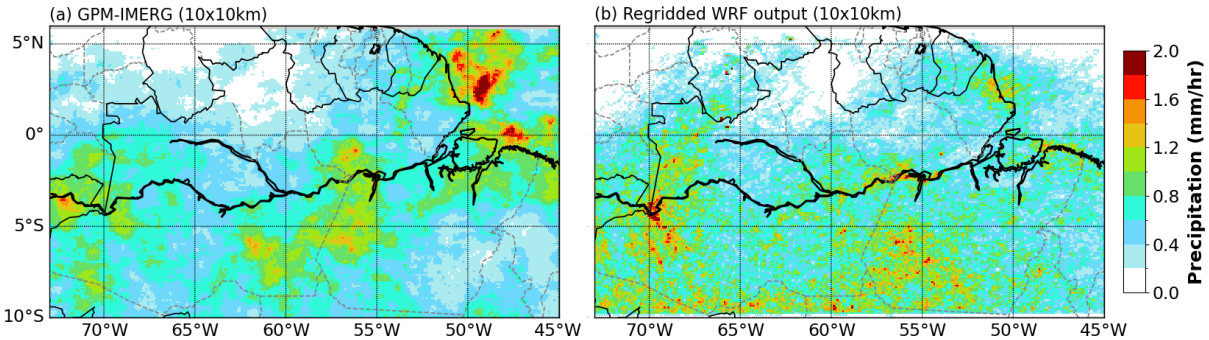

Figure S 6: Spatial distribution of mean precipitation (mm/h) for the period 11–30 January 2023, regridded to a 10×10 km resolution for intercomparison. Left: GPM satellite-derived precipitation. Right: WRF simulation.

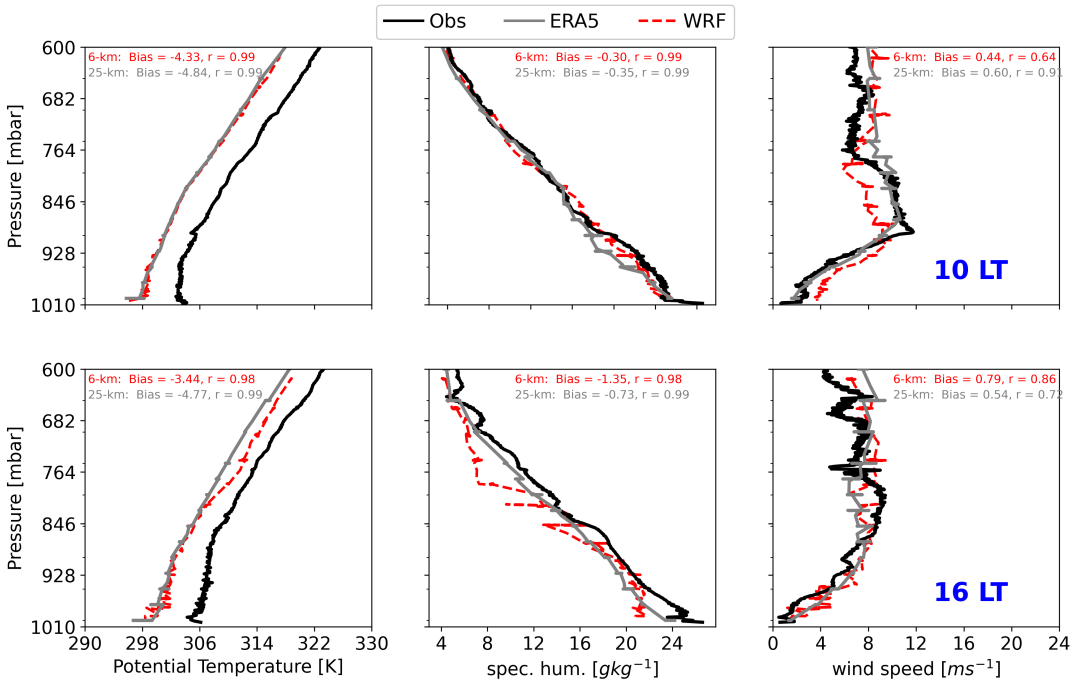

Figure S 7: Vertical profiles of potential temperature (left), specific humidity (middle), and wind speed (right) at 14 UTC (top row) and 20 UTC (bottom row). Observations from radiosondes are shown in black, ERA5 reanalysis in gray, WRF simulations in dotted red.

Table S 3: Statistical comparison of observed and simulated hourly data from the CAFE-Brazil flight on 14 January 2023.

	Potential Temperature (K)	**Specific Humidity (g/kg)**	**Wind Speed (m/s)**	**Vertical Velocity (m/s)**
Pearson (r)	0.99	0.98	0.75	-0.11
MB	-0.90	0.93	-0.58	0.40
RMSE	3.25	1.93	3.08	1.23

B.2 Evaluation of WRF-GHG tracer simulations against in-situ observations

Table S 4: Set of VPRM parameters used in the VPRM-Default and VPRM-optimized simulations

	T_{min}	T_{opt}	T_{max}	**Default**				**Calibrated (Botía et al., 2025)**			
				λ	PAR_0	α	β	λ	PAR_0	α	β
EF=1	0	20	40	-0.2101	501	0.1601	0	-0.1096	993.9	0.2114	1.8187
DF=2	0	20	40	-0.1729	324	0.3258	0	-0.1729	324	0.3258	0
MF=3	0	20	40	-0.2555	206	0.3422	0	-0.2555	206	0.3422	0
SHR=4	2	20	40	-0.0874	303	0.0239	0	-0.0874	303	0.0239	0
SAV=5	2	20	40	-0.1141	682	0.0049	0	-0.0277	6860.7	-0.2535	7.1125
CRO=6	-5	22	40	-0.1209	646	0.0043	0	-0.0417	2329	-0.0814	3.6716
GRA=7	2	18	40	-0.1334	157	0.0269	0	-0.0568	15475.5	-0.3122	7.3377
others=8	0	0	40	0	0	0	0	0	0	0	0

Table S 5: Biomas for the VPRM classes

VPRM Classes	(1) Evergreen	(2) Deciduous	(3) Mixed forest	(4) Shrubland	(5) Savannas	(6) Cropland	(7) Grassland	(8) Others
MapBiomas	- E. Needleleaf - E. Broadleaf	- D. Needleleaf - D. Broadleaf	- Mixed forest	- Closed Shrubland - Open Shrubland	- Woody Savannas - Savannas	- Croplands - Cropland and Vegetation	- Grassland	- Permanent Wetlands -Urban Snow and Ice Barren or Sparsely vegetated Water Bodies Lakes

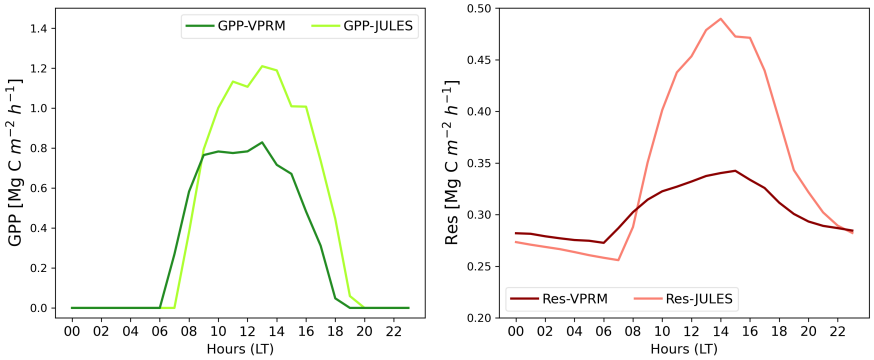

Figure S 8: Diurnal cycle of ecosystem carbon fluxes simulated by two models. Left panel: Gross Primary Productivity (GPP) from VPRM (dark green line) and JULES (light green line). Right panel: Ecosystem respiration (Res) from VPRM (dark red line) and JULES (salmon line).

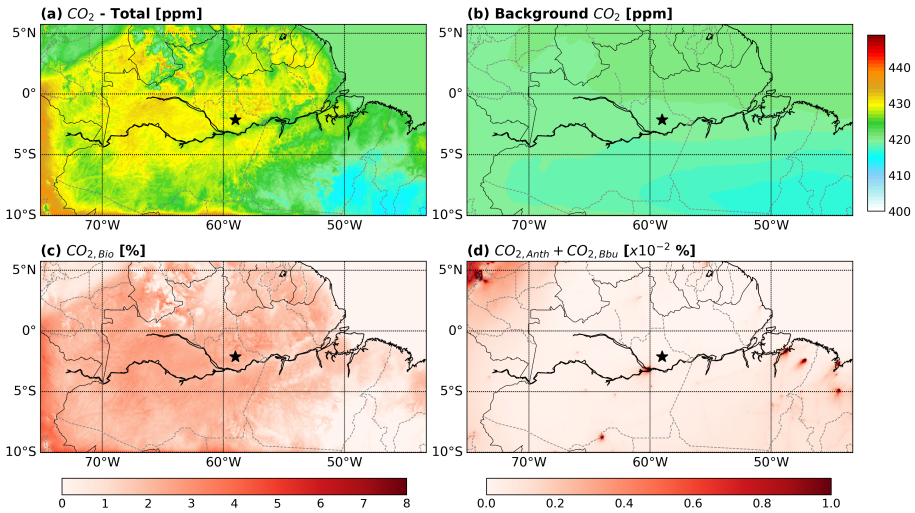

Figure S 9: Spatial distribution of total and source-partitioned carbon dioxide (CO_2) concentration simulated with the WRF-GHG model extracted at 81 meters. The panels show CO_2 total concentration (top-left), background CO_2 concentration (top-right), biogenic CO_2 (bottom-left) and anthropogenic + biomass burning CO_2 (bottom-right). Stars indicate the ATTO site location.

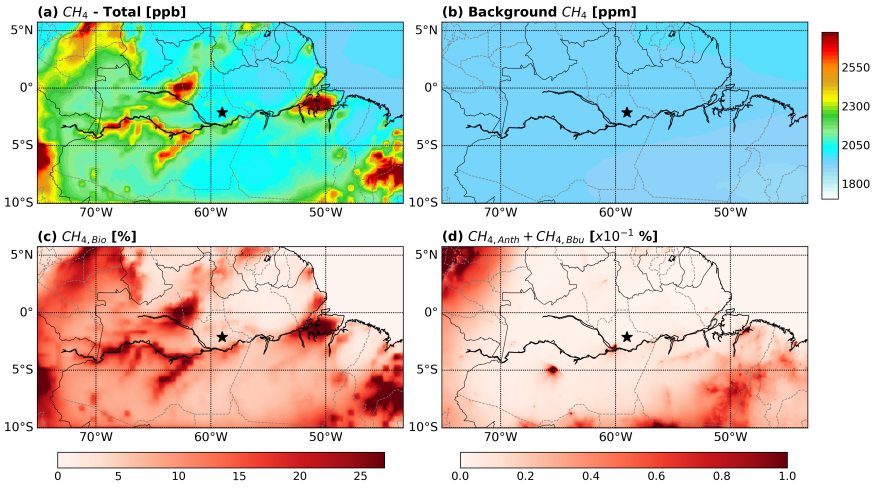

Figure S 10: Spatial distribution of total and source-partitioned methane (CH_4) concentration simulated with the WRF-GHG model extracted at 81 meters. The panels show CH_4 total concentration (top-left), background CH_4 concentration (top-right), biogenic CH_4 (bottom-left) and anthropogenic + biomass burning CH_4 (bottom-right). Stars indicate the ATTO site location.

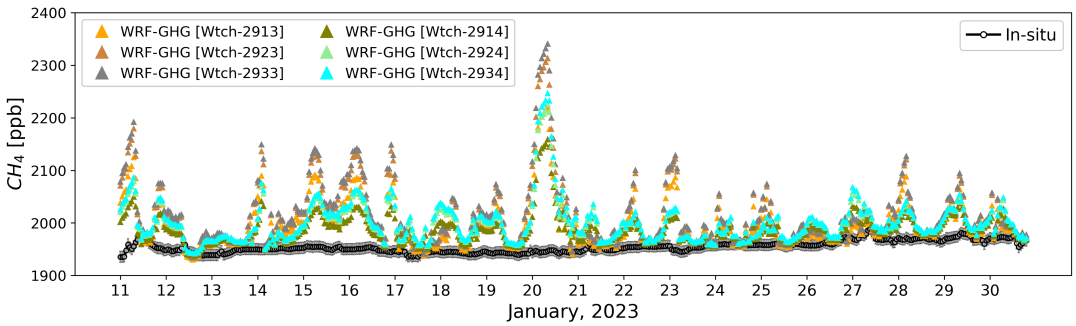

Figure S 11: Time series of total CH_4 concentration at INSTANT tower during January 2023, comparing observations (black circles) with simulations using Six-Model WetCharts ensemble for wetland fluxes.

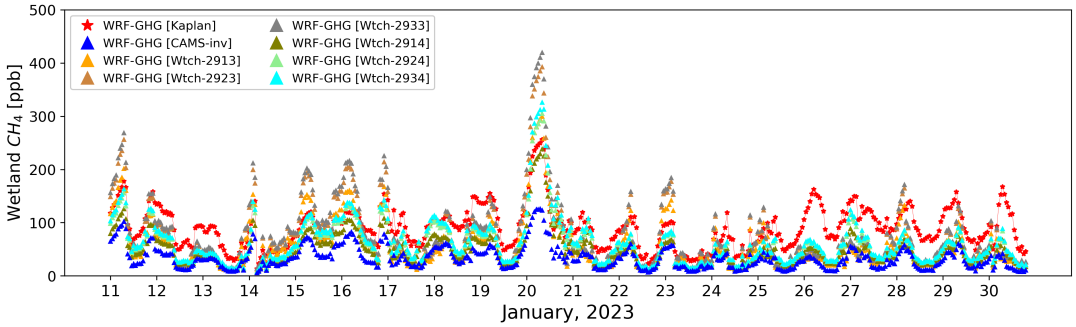

Figure S 12: Temporal variability of simulated CH_4 concentrations from wetlands sources over the Instant tower during January 2023, as represented by three emission inventories: Kaplan (red stars), CAMS-Inversion (blue triangles), and the Wetcharts ensemble (Wetch-2913 to Wetch-2934; colored triangles).

Figure S13 illustrates the CH_4 biogenic fluxes, advection patterns, and in-situ measurements at the ATTO Tower in January 2023. Panel (a) shows the CH_4 fluxes around ATTO, a selected region within D02, where biogenic methane sources could have a more significant impact on the ATTO area, with higher fluxes indicated by warmer colors. The region around the ATTO Tower is highlighted with a red box, showing significant flux variations. On the right side of the panel, a mask of CH_4 emission sources is provided, where areas in red represent regions with higher emissions, and areas in blue indicate lower emissions, with the ATTO Tower marked by a star. Panel (b) presents the advection patterns for two time periods: daytime (08:00–18:00 LT) on the left and nighttime (19:00–07:00 LT) on the right. The advection is shown in terms of ppb s^{-1}, with red and blue colors reflecting the movement of CH_4 towards and away from the tower, respectively, while the black arrows indicate the mean wind direction. Panel (c) displays the wind vectors and the transport of CH_4 towards the ATTO Tower during the day and night. The wind vectors are overlaid with shading that indicates the strength of CH_4 transport, where red shows CH_4 moving towards the tower and blue indicates movement away from it. The color bar shows wind speed in m/s. Finally, panel (d) provides a time series of simulated CH_4 concentrations at the ATTO Tower (black dashed line) and from a river source (red line) throughout January 2023, showing the fluctuations in CH_4 levels influenced by biogenic emissions at the tower and nearby river sources. This figure provides a detailed view of the regional CH_4 dynamics, highlighting the contribution of biogenic fluxes, wind patterns, and the advection of CH_4 to the ATTO Tower site.

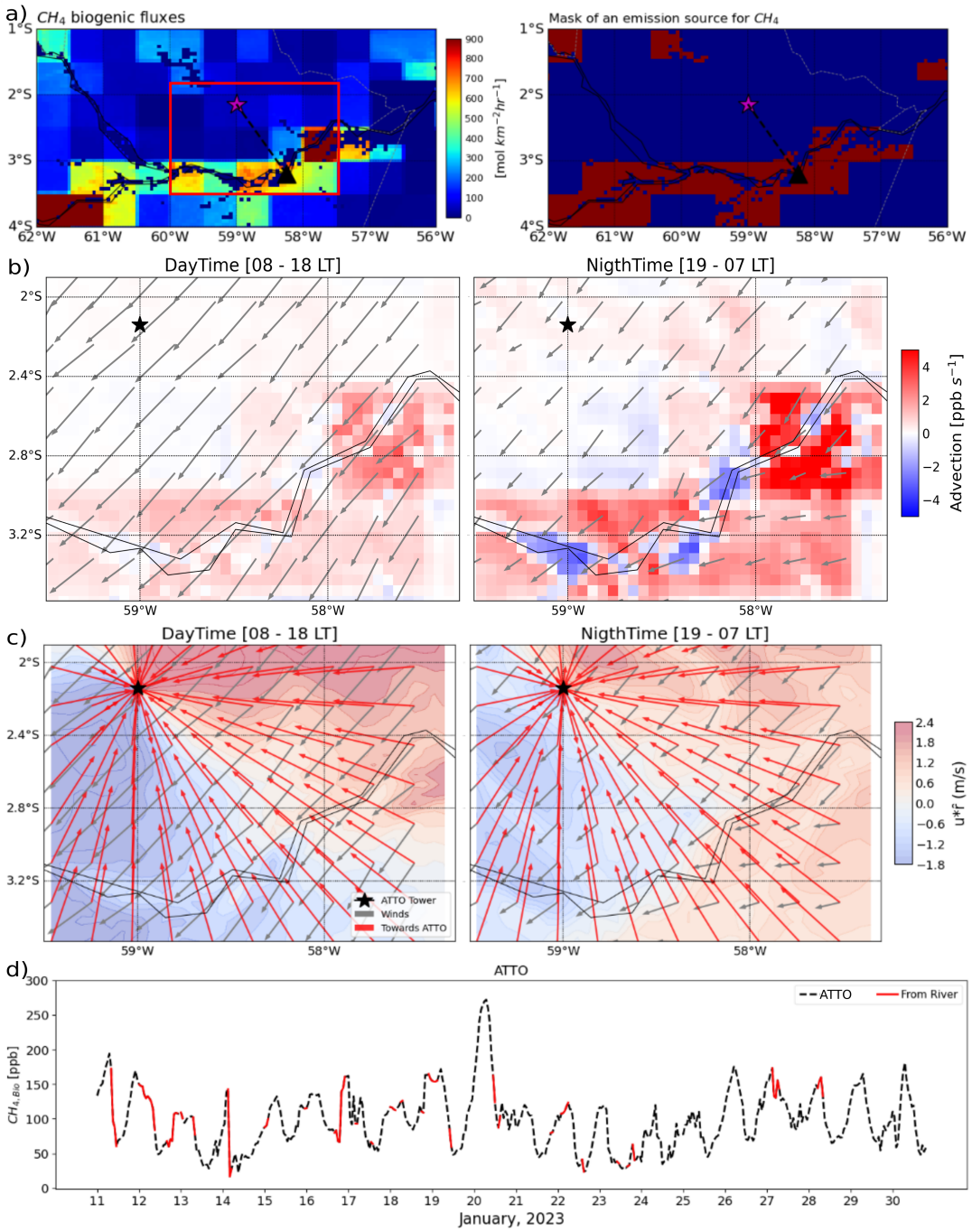

Figure S 13: CH_4 biogenic fluxes, advection patterns, and in-situ measurements at the ATTO Tower in January 2023. (a) CH_4 fluxes (left) and mask of a CH_4 emission source (right) in the study region. (b) Advection patterns for daytime (08:00-18:00 LT) and nighttime (19:00-07:00 LT). (c) Wind vectors and CH_4 transport towards the ATTO Tower during the day and night. (d) Time series of simulated biogenic CH_4 concentrations at the ATTO Tower (black dashed line) and from the river source (red line).

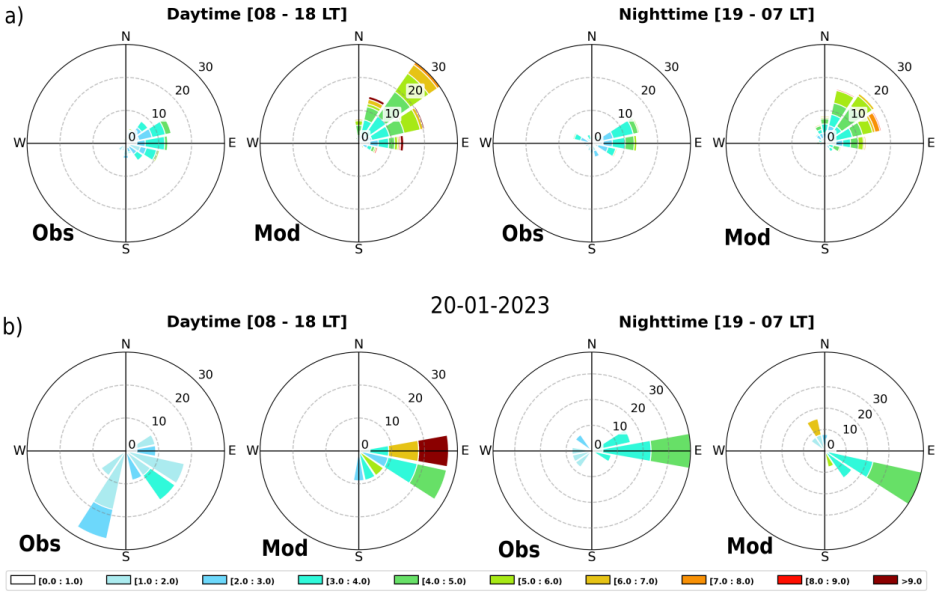

Figure S 14: Wind rose charts showing the wind fields during the daytime and nighttime: (a) for January 2023, and (b) for January 20, 2023, when the model simulated a peak in CH_4 concentrations.

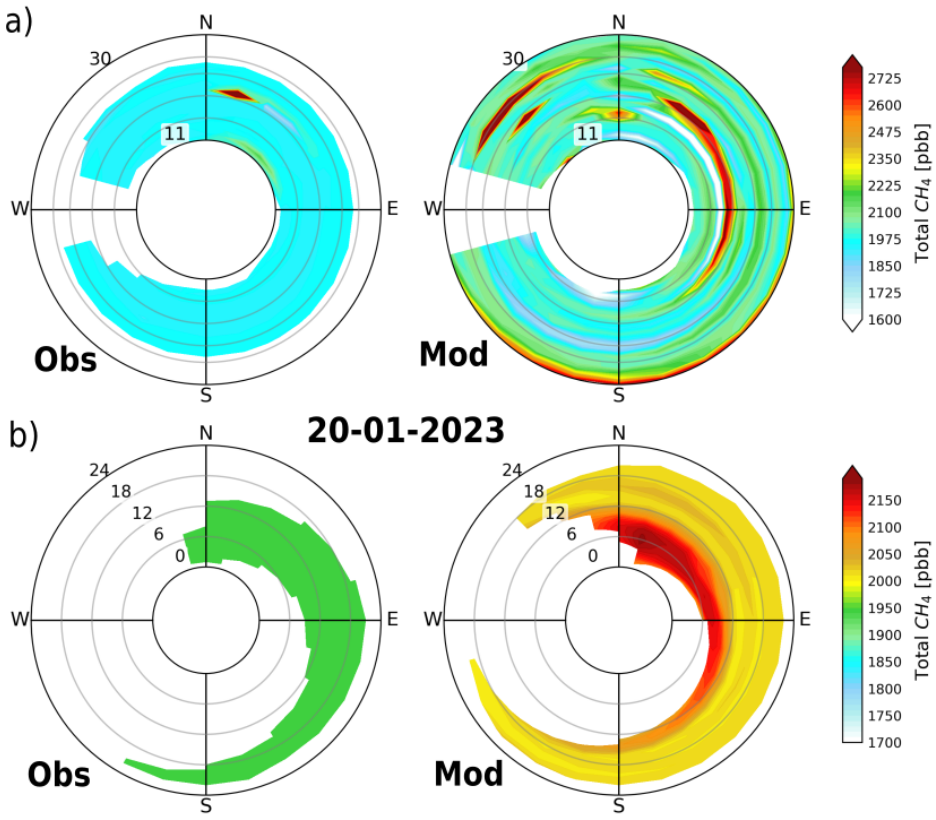

Figure S 15: Wind rose charts showing observed (left) and simulated (right) CH_4 concentrations at the ATTO site for (a) January 2023, and (b) January 20, 2023. The simulated data were considered by the Kaplan inventory.

C WRF-GHG simulation set-up

A detailed description on how to run WRF-GHG can be found in Beck et al., (2011); here, only the initialization procedure specific to our study is summarized. Typically, a daily simulation with WRF-GHG is performed over a 30h period, including a 6h meteorological spin-up from 18:00 to 24:00 UTC of the previous day, followed by a 24h simulation of tracer transport for the actual simulation day (Beck et al., 2011). In our case, however, a 10-day spin-up was used, so daily simulations start from the last day of the spin-up. To avoid negative tracer values, a small constant offset is applied to the WRF boundary fields of biospheric CO_2 (= 400) and the soil sink CH_4 (=1.8) at the start of each run. This offset is later subtracted during post-processing.

Meteorological conditions are updated daily using external data (ERA5). Tracers for total and background CO_2 and CH_4 fluxes are initialized on the first day of the simulation period using CAMS-Inversion, along with the lateral boundary conditions of the outer domain (D01). For subsequent days, the tracers are taken from the final WRF output of the previous day, ensuring continuity of the simulation. The CO_2 tracer for VPRM and the CH_4 tracer for soil uptake are also initialized with a constant offset to prevent negative values caused by vegetation respiration (Beck et al., 2011). Other flux tracers are initialized daily using external data sources to provide updated emission information for each tracer.